A thermal model for static current characteristics of AlGaN/GaN high electron mobility transistors including self-heating effect

Yuancheng Chang,[a] Yimen Zhang, and Yuming Zhang
Key Lab of Ministry of Education for Wide Band-Gap Semiconductor Materials and Devices, Microelectronics Institute, Xidian University, Xi'an, Shaanxi 710071, China

K. Y. Tong
Department of Electronic and Information Engineering, The Hong Kong Polytechnic University, Hong Kong, China

A thermal model of AlGaN/GaN high electron mobility transistors (HEMTs) has been developed based on a quasi-two-dimensional numerical solution of Schrödinger's equation coupled with Poisson's equation. The static current characteristics of HEMT devices have been obtained with the consideration of the self-heating effect on related parameters including polarization, electron mobility, saturation velocity, thermal conductivity, drain and source resistance, and conduction-band discontinuity at the interface between AlGaN and GaN. The simulation results agree well with our experimental data. It has also been demonstrated that the reduction of the saturation drain current at high power dissipation is primarily due to the decrease of electron mobility in the channel. The proposed model is valuable for predicting and evaluating the performance of different device structures and packages for various applications. © *2006 American Institute of Physics.*
[DOI: 10.1063/1.2171776]

I. INTRODUCTION

With the great progress of the AlGaN/GaN high electron mobility transistor (HEMT) in recent years, it has become a promising candidate to operate at high frequency, high power, and high temperature and attracted much research. Many AlGaN/GaN HEMT devices fabricated either on sapphire or SiC substrates have been demonstrated.[1–5] They have shown excellent performances for the applications to the future microwave systems.

However, the high power dissipation of AlGaN/GaN HEMTs operating at large biases may result in high junction temperature and enhance the phonon scattering causing a drop of carrier mobility. This effect has been reported to be of great influence on the static current characteristics, and is commonly referred to as "self-heating." The evidence of such an effect is a negative slope of drain current I_{ds} versus drain voltage V_{ds}. The self-heating effect may degrade the gate electrode due to the accelerated electromigration, and can easily burn metal wires connecting the chip to the package, thus causing device failures and reliability problems. Severe self-heating may even damage the device itself.[6,7] Nuttinck *et al.* measured the *I-V* characteristics of an AlGaN/GaN HEMT device under the pulse and also continuous bias conditions at different temperatures. These measurements gave an in-depth understanding of the self-heating effect.[8] Park *et al.* introduced a thermal model.[9] In their computation, the PAMICE code was used to calculate the temperature, and a nematic liquid-crystal thermograph was adopted to evaluate the peak temperature on the surface of the device chip. In addition, Gaska *et al.* compared the self-heating effect in AlGaN/GaN HEMT devices grown on sapphire and

SiC substrates.[10] Their results demonstrate that HEMTs with SiC substrates have superior electron-transport properties and are more suitable for high power electronic applications.

Our work is focused on the generation of the self-heating in AlGaN/GaN HEMTs and its influence on the channel current as well as the relationship between the self-heating and device structure. In this paper, Sec. II presents a self-consistent scheme to determine the electron-density distribution at the interface between AlGaN and GaN. A quasi-two-dimensional approach to calculate the channel current is proposed in Sec. III. Section IV shows a comparison of the simulation results with the experimental data. A conclusion is drawn in Sec. V.

II. MODEL DESCRIPTION

In order to study the operational mechanisms of high electron mobility transistors based on the AlGaN/GaN heterojunction structure, Schrödinger's equation is used in a self-consistent approach coupled with Poisson's equation.[11,12]

With the effective-mass theory, Schrödinger's equation takes the form,[13]

$$-\frac{\hbar^2}{2}\frac{d}{dz}\left[\frac{1}{m(z)}\frac{d}{dz}\right]\varphi + [eV(z) + \Delta E(z)]\varphi = E\varphi, \qquad (1)$$

where $m(z)$ is the position-dependent effective mass, $V(z)$ is the electrostatic potential, $\Delta E(z)$ is the band discontinuity at the heterojunction, φ is the electron wave function, and E is the electron energy.

In nitride semiconductors grown in the wurtzite structure, due to the presence of spontaneous and piezoelectric polarizations, the displacement field $D(z)$ is given by Poisson's equation as

[a]Electronic mail: changych@163.com

99, 044501-1

TABLE I. Fitting parameters of the Varshni equation for the variation of band gap with temperature.

	α(meV/K)	β(K)
GaN	−1.08	745
AlN	−1.799	1462

$$\frac{d}{dz}D(z) = \frac{d}{dz}\left[-\varepsilon(z)\frac{d}{dz}V(z) + P(z)\right]$$
$$= e[p(z) - n(z) + N_D^+ - N_A^-], \qquad (2)$$

where $\varepsilon(z)$ is the position-dependent dielectric constant, $P(z)$ is the total polarization, $n(p)$ is the electron (holes) concentration, and $N_D^+(N_A^-)$ is the ionized donor (acceptor) density.

A self-consistent scheme to solve the above equations by numerical methods has been set up, in which the potential V is obtained from Eq. (2) with an initial guess of the mobile charge density, and then inserted into Schrödinger's equation to solve the energy levels and the wave function of the quantum well. The electron density is calculated according to Fermi statistics

$$n(z) = \frac{m(z)k_BT}{\pi\hbar^2}\sum_i |\varphi_i(z)|^2 \ln[1 + e^{(E_F - E_i)/k_BT}], \qquad (3)$$

where E_F is the Fermi level, E_i is the energy of the ith quantized level, T is the temperature, and k_B is Boltzmann constant. The calculated electron density is then plugged into Poisson's equation again, and iteration is repeated until the convergence is achieved. This simple iteration by itself may not converge, so it is necessary to implement underrelaxation for the electron density with an adaptive relaxation factor ω. The exact value of ω is unknown in advance and it needs to be readjusted during the iteration.

The dependence of some important parameters on Al composition and temperature should be taken into account.

A. Energy-band offset

In many semiconductors including the nitrides, the empirical Varshni formula approximates well the observed temperature dependence of the band gap,[14]

$$E_g(T) = E_g(0) - \frac{\alpha T^2}{T + \beta}, \qquad (4)$$

where $E_g(0)$ is the energy gap at 0 K, α is an empirical constant and β sometimes associates with the Debye temperature. For GaN and AlN, there were a few reported measurements[14,15] as summarized in Table I.

In many cases, the following function form is suitable for the band gap of alloy $A_xB_{1-x}C$ (Ref. 16)

$$E_g(x) = xE_g^{AC} + (1-x)E_g^{BC} - bx(1-x), \qquad (5)$$

where x is the mole fraction of Al, and b is a bowing factor. Several theoretical calculations have been directed at the properties of the technologically important cation-substituted nitride alloys. Van Schilfgarde found $b=0.6$ for $Al_xGa_{1-x}N$, and so its band gap is[17]

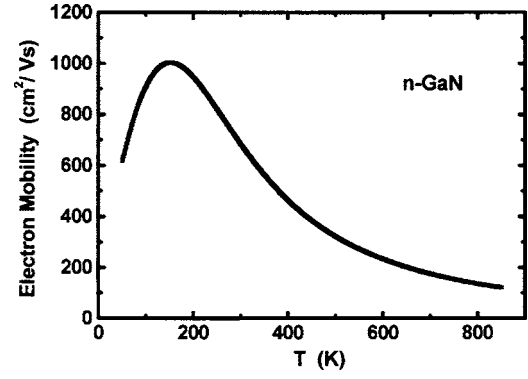FIG. 1. Calculated electron mobility vs temperature.

$$E_g^{AlGaN}(T,x) = xE_g^{AlN}(T) + (1-x)E_g^{GaN}(T) - bx(1-x). \qquad (6)$$

The conduction-band discontinuity ΔE_c at the $Al_xGa_{1-x}N/$GaN heterointerface is a principal parameter in determining the two-dimensional electron gas (2DEG) density. Generally, a higher 2DEG density can be attained with a larger ΔE_c. In $Al_xGa_{1-x}N/$GaN HEMTs, ΔE_c is assumed to be as follow[18]

$$\Delta E_c = 0.70[E_g^{AlGaN}(T,x) - E_g^{GaN}(T)]. \qquad (7)$$

B. Carrier mobility

A simple analytical model which has successfully described the mobility in SiC is utilized to characterize the low-field mobility in GaN in our simulation. This is based on the well-known Caughey-Thomas expression,

$$\mu_i(N) = \mu_{min,i} + \frac{\mu_{max,i} - \mu_{min,i}}{1 + (N/N_{g,i})^\gamma}. \qquad (8)$$

At low doping level and room temperature, phonon scattering is the major mechanism of scattering. The contribution from impurity scattering is obtained by subtracting the phonon contribution from the total mobility described above. So the Caughey-Thomas relation can be written in the following form:

$$\mu_i(N,T) = \mu_{max,i}(T_o)\frac{B_i(N)(T/T_o)^\xi}{1 + B_i(N)(T/T_o)^{\delta+\xi}}, \qquad (9)$$

where

$$B_i(N) = \left[\frac{\mu_{min,i} + \mu_{max,i}(N_{g,i}/N)^\gamma}{\mu_{max,i} - \mu_{min,i}}\right]\Bigg|_{T=T_o},$$

$i=n$ or p is for electrons and holes, respectively, N is the doping concentration, and $T_0=300$ K. The parameters $\mu_{max,i}$, $\mu_{min,i}$, $N_{g,i}$, γ, δ, and ξ depend on the type of semiconductor material and their values are taken from Ref. 19.

Figure 1 shows the calculated temperature dependence of mobility in wurtzite GaN with parameter values from Table II. It can be seen that at low temperature, the increase of mobility versus temperature is mainly due to the contribution from the ionized impurity scattering. However, the mobility drops because of the phonon scattering when the temperature is increased.

TABLE II. The values of the parameters.

$\mu_{max,i}$ (cm^2/V s)	$\mu_{min,i}$ (cm^2/V s)	$N_{g,i}$ (cm^{-3})	γ	δ	ξ
1000	55	2×10^{17}	1.0	2.0	0.7

C. Spontaneous and piezoelectric polarizations

The spontaneous polarization of $Al_xGa_{1-x}N$ is given to second order of x by[20]

$$P_{AlGaN}^{sp}(x) = -0.090x - 0.034(1-x)$$
$$+ 0.021x(1-x)(C/m^2). \quad (10)$$

The first two terms in Eq. (10) are the usual linear interpolation between binary compounds. The third term is the so-called bowing, embodying nonlinearity of quadratic order. Higher-order terms are ignored as their effect is estimated to be less than 10%.[21] Although the spontaneous polarization is very strong in group III nitrides, the pyroelectric coefficients describing the change of spontaneous polarization with temperature are measured to be surprisingly small. We have adopted the recent data $dP/dT = 7.5 \ \mu C/Km^2$ (Ref. 20) for AlN and $dP/\varepsilon dT \sim 10^4$ V/mK (Ref. 22) for GaN (where ε is the static dielectric permittivity).

The piezoelectric polarization in the direction of c axis is specified as

$$P_{pz} = 2\frac{a - a_0}{a_0}\left(e_{31} - e_{33}\frac{C_{13}}{C_{33}}\right). \quad (11)$$

With the linear interpolation of elastic and piezoelectric constants, the piezoelectric polarization from Eq. (11) is nonlinear with alloy composition. This can be approximated by the following quadratic equation with an error less than 1%:[20]

$$P_{AlGaN/GaN}^{pz}(x) = -0.0525x + 0.0282x(1-x)(C/m^2). \quad (12)$$

There have been no reports on the temperature dependence of piezoelectric polarization. We have neglected the temperature dependence of piezoelectric polarization since it is predicted to be very small.

The total polarization of an AlGaN layer is the sum of spontaneous polarization and piezoelectric polarization in the equilibrium state. For GaN, a value of -0.029 C/m^2 is used as its spontaneous polarization at room temperature.[23]

D. Saturation velocity

The saturation velocity is described with an empirical temperature function derived from fitting the results of Monte Carlo simulation,[24]

$$v_{sat} = 2.87 \times 10^7 - 9.8 \times 10^3 \times T \ (cm/s). \quad (13)$$

At a high electric field, it is found that the saturation velocity is weakly dependent on the temperature.

E. Thermal conductivity

We are not able to find an analytical expression for the thermal conductivity of GaN from the literatures. However, an empirical fitting power law can be applied[25]
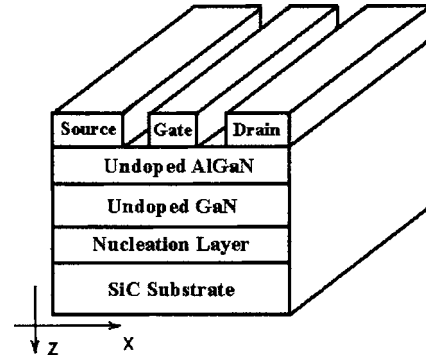

FIG. 2. The Structure of the HEMT with Al mole fraction of 0.3.

$$K_{GaN}(T) = 1.6\left(\frac{T}{300}\right)^{-1.4} \ (W/cm \ K). \quad (14)$$

At present, the AlGaN/GaN HEMT devices are fabricated either on SiC or on sapphire substrates. In the case of SiC, it has a relatively high thermal conductivity as shown in Ref. 26,

$$K_{SiC}(T) = 3.4\left(\frac{T}{300}\right)^{-1.5} \ (W/cm \ K). \quad (15)$$

F. Drain and source resistances

The drain and source resistances consist of two parts: the bulk resistance in the active area and the ohmic contact resistance. However, the ohmic contact resistance mainly depends on the tunneling effect that is hardly affected by temperature. The bulk resistances are defined by

$$R_{db} = \frac{L_{gd}}{qN_D^+Wa\mu_n}, \quad R_{sb} = \frac{L_{gs}}{qN_D^+Wa\mu_n}. \quad (16)$$

So the drain and source resistances are written as

$$R_d = R_{ohm} + R_{db}, \quad R_s = R_{ohm} + R_{sb}, \quad (17)$$

where L_{gs} and L_{gd} are the distances from gate to source and gate to drain, respectively, W is the width of the gate, and a is the thickness of the channel.

III. CURRENT MODEL

A quasi-two-dimensional model has been utilized for the calculation of I-V characteristics of an AlGaN/GaN HEMT device. This makes use of the exact value of the sheet charge density of the channel, which is derived from the solution of Schrödinger's and Poisson's equations presented above. The device structure is shown in Fig. 2 where the x axis is the direction along the channel, V_x is the voltage in x direction, and the z axis is perpendicular to the channel. When a drain bias is applied, the sheet electron charge density is determined by

$$n_s(V_x) = \int n(V_x,z)dz. \quad (18)$$

Neglecting diffusion component, the drain current I_{ds} is

$$I_{ds} = -qW\nu(E)n_s(x). \tag{19}$$

$\nu(E)$ is the mean electron velocity which can be expressed by

$$\nu(E) = \frac{\mu_0 E}{1 + E/E_c}, \tag{20}$$

where μ_0 is the low-field mobility, E_c is the critical electric field, and $E_c = \nu_{sat}/\mu_0$, ν_{sat} is the saturation velocity.[13]

The numerical solution is based on the discretization of Eq. (19) by dividing the channel length into N sections, with each section having a length of h, so that $Nh = L_g$. Let V_i, V_{i-1} express the potentials across the ith section. Therefore $V_i = V_{i-1} + E_i h$, where E_i is the horizontal electric field in the ith section. By solving iteratively for all the N sections, we can obtain the value of the voltage V_d across the channel which is consistent with an assumed current I_{ds}. Parasitic components are included explicitly in terms of the values of R_d and R_s, so the voltage V_{ds} between the source and the drain is given by

$$V_{ds} = V_d + (R_d + R_s)I_{ds}. \tag{21}$$

During the calculation the self-heating effect has been taken into account as follows. The temperature difference between the channel and the bottom of the substrate ($\Delta T = T_{channel} - T_{sub}$) is[27]

$$\frac{\Delta T}{T_{sub}} = \frac{1 - (1 - P_{diss}/4P_0)^4}{(1 - P_{diss}/4P_0)^4}, \tag{22}$$

where $T_{channel}$ is the channel temperature and T_{sub} is the temperature of the substrate bottom. P_0 is referred to as a characterization quantity with the dimension of power

$$P_0 = \frac{\pi K(T_{sub})WT_{sub}}{\ln(8t_{sub}/\pi L_g)}, \tag{23}$$

where $P_{diss} = I_{ds}V_{ds}$ is the power dissipation, $K(T_{sub})$ is the thermal conductivity, t_{sub} is the thickness of substrate, and L_g is the length of the gate.

The initial value of V_{ds} is evaluated for a given I_{ds}, then ΔT and other parameters at this temperature are calculated from Eqs. (4)–(17). Repeating similar steps for a certain range of I_{ds}, the corresponding values of V_{ds} and the I-V characteristics of device are achieved.

In addition, the following two assumptions are applied:

(a)   The HEMT structure includes two parts: the epitaxial layers and the substrate. In each part, the temperature changes smoothly.

(b)   The bottom temperature of the substrate T_{sub} increases linearly with the dissipated power,

$$T_{sub} = 300 + \lambda P_{diss}, \tag{24}$$

where λ is an empirical parameter corresponding to the thermal resistance of the package.

IV. SIMULATION RESULTS AND DISCUSSION

An $Al_xGa_{1-x}N/GaN$ HEMT with $L_g = 0.8$ μm and $W = 94$ μm is utilized to verify our model. The structure of the device is i-$Al_xGa_{1-x}N$ (30 nm)/i-GaN(3 μm)/low-temperature nucleation layer/i-SiC(300 μm),[28] as shown in
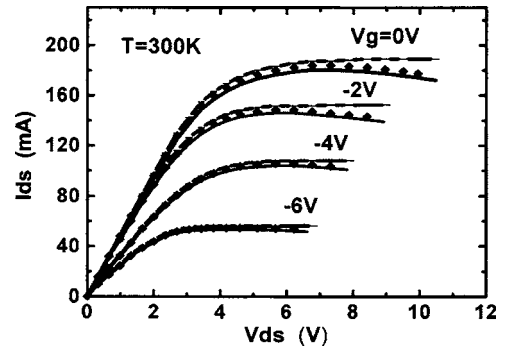

FIG. 3. A comparison between experimental data (square) and simulated I-V characteristics with self-heating effect (line) and without self-heating effect (dash line) at various gate biases. The experimental data are from Ref. 28.

Fig. 2. In our calculation a Schottky barrier height of $\varphi_B = 1.3x + 0.85$ eV (Ref. 29) is used for the $Pt/Au - Al_xGa_{1-x}N$ contact, where x is mole fraction of Al. When $x = 0.3$, the barrier height is 1.24 eV. The effective mass in our calculation is 0.19 for electrons in both GaN and $Al_xGa_{1-x}N$. Also the static dielectric constant $\varepsilon_r = 9.7 - 1.2x$ is used with L_{gs} and L_{gd} at 1.8 and 2.4 μm, respectively.

The temperature difference ΔT is obtained from Eqs. (22) and (23). It is as high as 86.7 K when the drain current reaches saturation at a gate voltage of 0 V. The electron mobility in the channel drops drastically from 685 to 480 cm²/V s by about 29.9%. The band offset and saturation velocity are weakly dependent on the temperature, and remain almost constant while the temperature increases. Although the spontaneous polarization is very strong in the group III nitrides, the changes of spontaneous polarization with temperature are only 0.29% and 0.56% for GaN and $Al_xGa_{1-x}N$, respectively, because the pyroelectric coefficients are measured to be very small. A specific ohmic contact resistance of about 2 Ω mm is taken to be accordant with the measured values of these devices.[30] The bulk resistances R_{sb} and R_{db} increase from 0.35 and 0.46 Ω to 0.49 and 0.66 Ω, respectively.

Figure 3 shows a comparison of the calculated I-V characteristics with the experimental data for the cases with and without the self-heating effect. A good agreement is achieved between the simulated results with self-heating and the experimental measurements. This is contributed to the fact that a relatively accurate model is used and an empirical parameter λ is adopted. The value of λ is about 5 K/W. From Fig. 3 it can be immediately noticed that the current declines while the voltage increases for higher dissipated power. This means that the self-heating effect becomes more serious at these conditions. But the negative slope of the current recedes as the dissipated power is low. It can be also seen that there is a great deviation between the experimental and theoretical results without the self-heating effect. This discrepancy implies that the electron current in the channel depends strongly on temperature. The increased drain voltage results in more dissipated power and leads to higher channel temperature. This causes a reduction in electron mobility and decreases the drain current.

In our simulation, we have overlooked the influence of

temperature on piezoelectric polarization at the heterointerface between $Al_xGa_{1-x}N$ and GaN. Actually the rise of temperature may enhance piezoelectric effects and increases the value of n_s. Thus the calculated current is slightly smaller than the experimental values.

V. CONCLUSIONS

The static current characteristics of an AlGaN/GaN HEMT have been obtained by means of a quasi-two-dimensional approach. The simulation results based on the self-heating effect agree well with the experimental data. The high power dissipation in the device induces an obvious self-heating effect even though GaN material has good thermal conductivity. This phenomenon possibly lowers the current drive capability of the device. The presented results also indicate that the reduction of saturation drain current at high power region is primarily due to the decrease of electron mobility in the channel. Therefore it is important for a designer to take this effect into account in device design and calculation.

ACKNOWLEDGMENTS

[1] A. Kuliev, V. Kumar, R. Schwindt, D. Selvanathan, A. M. Dabiran, P. Chow, and I. Adesida, Solid-State Electron. **47**, 117 (2003).

[2] U. K. Mishra, P. Parikh, and Y. F. Wu, Proc. IEEE **90**, 1022 (2002).

[3] P. Javorka, A. Alam, M. Wolter, A. Fox, A. M. Marso, H. Luth, and P. Kordos, IEEE Electron Device Lett. **23**, 4 (2002).

[4] Y. F. Wu, D. Kapolnek, J. P. Ibbetson, P. Parikh, B. P. Keller, and U. K. Mishra, IEEE Trans. Electron Devices **48**, 586 (2001).

[5] M. Kuball, J. M. Hayes, M. J. Uren, and T. Martin, IEEE Electron Device Lett. **23**, 7 (2002).

[6] J. Park, M. W. Shin, and G. C. Lee, IEEE Trans. Electron Devices **51**, 1753 (2004).

[7] S. Nuttinck, B. K. Wangner, B. Banerjee, S. Venkataraman, E. Gebara, J. Laskar, and H. M. Harris, IEEE Trans. Microwave Theory Tech. **51**, 2445 (2003).

[8] S. Nuttinck, E. Gebara, J. Laskar, and H. M. Harris, IEEE Trans. Microwave Theory Tech. **49**, 2445 (2001).

[9] J. Park, M. W. Shin, and C. C. Lee, IEEE Electron Device Lett. **24**, 424 (2003).

[10] R. Gaska, A. Osinsky, J. W. Yang, and M. S. Shur, IEEE Electron Device Lett. **19**, 89 (1998).

[11] R. Cingolani, A. Botchkarev, H. Tang, and H. Morkoc, Phys. Rev. B **61**, 2711 (2000).

[12] F. Della Sala, A. Di Carlo, P. Lugli, F. Bernardini, V. Fiorentini, R. Scholz, and J. M. Jancu, Appl. Phys. Lett. **74**, 2002 (1999).

[13] F. Sacconi, A. Di Carlo, P. Lugli, and H. Morkoc, IEEE Trans. Electron Devices **48**, 450 (2001).

[14] H. Teisseyre, P. Perlin, T. Suski, A. Pietraszko, and T. D. Moustakas, J. Appl. Phys. **76**, 2429 (1994).

[15] Q. Guo and A. Yoshida, Jpn. J. Appl. Phys., Part 1 **33**, 2453 (1994).

[16] A. Sher, M. van Schilfgaarde, M. A. Berding, S. Krishnamurthy, and A. B. Chen, MRS Internet J. Nitride Semicond. Res. **4S1**, G 5.1 (1999).

[17] M. van Schilfgaarde, A. Sher, and A. B. Chen, J. Cryst. Growth **178**, 8 (1997).

[18] G. Martin, A. Botchkarev, A. Rockett, and H. Morkoc, Appl. Phys. Lett. **68**, 2541 (1996).

[19] T. T. Mnatsakanov, M. E. Levinshtein, L. I. Pomortseva, S. N. Yrukov, G. S. Simin, and M. A. Khan, Solid-State Electron. **47**, 111 (2003).

[20] O. Ambacher *et al.*, J. Phys.: Condens. Matter **14**, 3399 (2002).

[21] V. Fiorentini, F. Bernardini, and O. Ambacher, Appl. Phys. Lett. **80**, 1204 (2002).

[22] M. S. Shur, A. D. Bykhovski, and R. Gaska, MRS Internet J. Nitride Semicond. Res. **4S1**, G1.6 (1999).

[23] O. Ambacher *et al.*, J. Appl. Phys. **85**, 3222 (1999).

[24] G. E. Bunea, S. T. Dunham, and T. D. Moustakas, MRS Internet J. Nitride Semicond. Res. **4S1**, G6.41 (1999).

[25] J. C. Freeman, IEEE MTT-S Int. Microwave Symp. Dig. **3**, 2031 (2004).

[26] A. S. Royet, T. Ouisse, B. Cabott, O. NOblanc, and C. Amodo, IEEE Trans. Electron Devices **47**, 2221 (2000).

[27] P. C. Canfield, S. C. F. Lam, and D. J. Allstot, IEEE J. Solid-State Circuits **25**, 299 (1990).

[28] J. Park, C. C. Lee, J. W. Kim, J. S. Lee, W. J. Hwang, and M. W. Shin, Phys. Status Solidi C **7**, 2364 (2003).

[29] O. Ambacher *et al.*, J. Appl. Phys. **87**, 334 (2000).

[30] M. Akita, S. Kishimoto, and T. Mizutani, IEEE Electron Device Lett. **22**, 376 (2001).